JOURNAL OF APPLIED ELECTROCHEMISTRY 12 (1982) 449–461

Current-time behaviour for copper electrodeposition. II. Experimental examination of surface diffusion and direct incorporation models at hemispherical sites

Y. OGATA*, K. YAMAKAWA, S. YOSHIZAWA

Department of Industrial Chemistry, Kyoto University, Kyoto, Japan

Received 16 October 1981

The surface diffusion model has been examined by the measurement of current–time transients for copper electrodeposition on to a polycrystalline copper electrode in acidic copper sulphate solution. The results did not satisfy the surface diffusion model criteria. The current–time profiles showed a linear dependence on $1/t^{1/2}$ except at high overpotentials. This behaviour could be explained by a direct incorporation model at hemispherical sites through a hemispherical diffusion layer. A parameter characterizing this model, the number of sites, was estimated to be of the order of 10^4 cm^{-2}.

1. Introduction

During potentiostatic electrodeposition, one can monitor the variation of current with time. The behaviour appears not only in the diffusion-controlled potential region but also at lower overpotentials. The cause of this behaviour has been considered to be a result of an increase in the surface area of the electrode [1, 2], a change in the activity of the electrode (which is related to the ratio of the preferred planes appearing on the electrode surface during electrodeposition [3]) and/or the surface diffusion effect [4–7]. Under limiting current conditions, the current–time behaviour, in the range of seconds or longer, is supposed to result from one of the first two effects. For shorter time periods, surface diffusion determines the current. The current–time behaviour for copper electrodeposition has been analysed theoretically in a previous paper [8].

In the present study, the analysis is compared with experimental results obtained from potentiostatic copper electrodeposition from acidic copper sulphate solution and another model must be proposed. Polycrystalline copper was used as the electrode. This is utilized industrially and studies using polycrystalline materials are apt to be orientated towards the technological viewpoint. On the other hand, there are studies using well defined conditions, namely, single crystals and even single crystals without dislocations, as the electrode. The two kinds of study do not seem to be satisfactorily related. The present study aims to bridge the gap between them using materials of the former type of study, and techniques and theories of the latter type.

2. Experimental details

2.1. *Electrodes and solutions*

Cold-rolled polycrystalline copper, of purity 99.9%, was utilized for the electrodes. A copper disc was first mechanically polished, then electropolished in 50 vol% aqueous phosphoric acid at 0.5 A cm^{-2} for 4 min and rinsed with triple-distilled water before being used as an electrode. Solutions of 0.5 mol dm^{-3} $CuSO_4$ + 2.0 mol dm^{-3} H_2SO_4 and 0.05 mol dm^{-3} $CuSO_4$ + 0.5 mol dm^{-3} H_2SO_4 were used. They were prepared using reagent grade materials and triple-distilled water.

* Present address: Department of Synthetic Chemistry, Nagoya Institute of Technology, Gokiso-cho, Showa-Ku, Nagoya 466, Japan.

0021-891X/82/040449-13$04.06/0

2.2. *Electrolytic cell and procedures*

A schematic view of the cell used is shown in Fig. 1. The material used was Teflon. A copper plated copper rod was used as a reference electrode. The electrode showed very stable potentials and its potential was measured versus the Hg/Hg_2SO_4 electrode. A copper plated platinum disc was used as a counter electrode in order to avoid a concentration change of copper ion during electrolysis.

A continuous potential pulse (15 ms duration, 1 : 1 duty ratio) was applied and the current–time response (current transient) was measured using an oscilloscope. The experiments were performed at room temperature and in an argon atmosphere.

3. Results and discussion

3.1. *The surface diffusion model*

Typical current–time responses on applying a potentiostatic pulse are shown in Fig. 2. The results in 0.5 mol dm^{-3} $CuSO_4$ + 2.0 mol dm^{-3} H_2SO_4 are replotted as i/i_∞ in Figs. 3 and 4 according to the theoretical treatment given for the surface diffusion model in a previous paper [8]. The time range measured may not be long enough compared with the theoretical curves. However, it is possible to regard the experimental curves as corresponding to the bottom part of the theoretical ones. This gives us the corresponding N_2 values from the experimental data. N_2 is a function as defined in Equation 1 (the notation of this section is the same as in the previous paper).

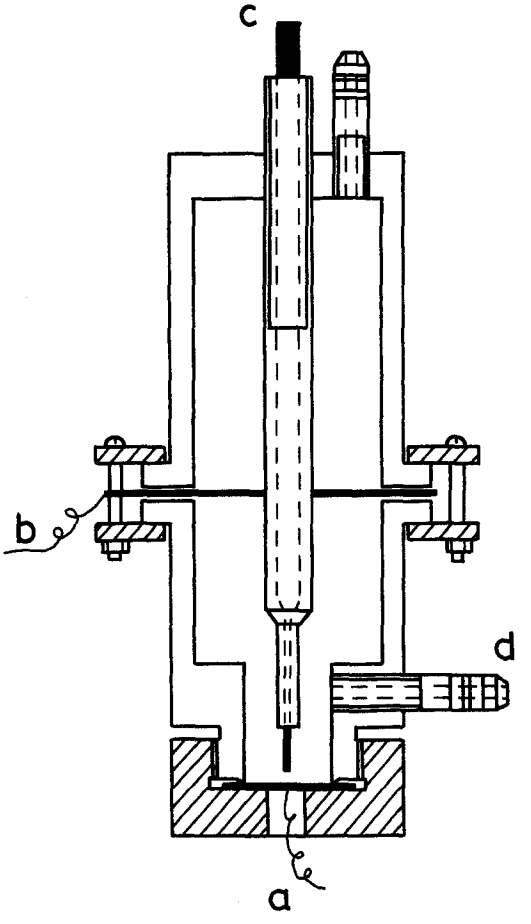

Fig. 1. Electrolytic cell. a: working electrode, b: counter electrode, c: reference electrode, d: gas inlet.

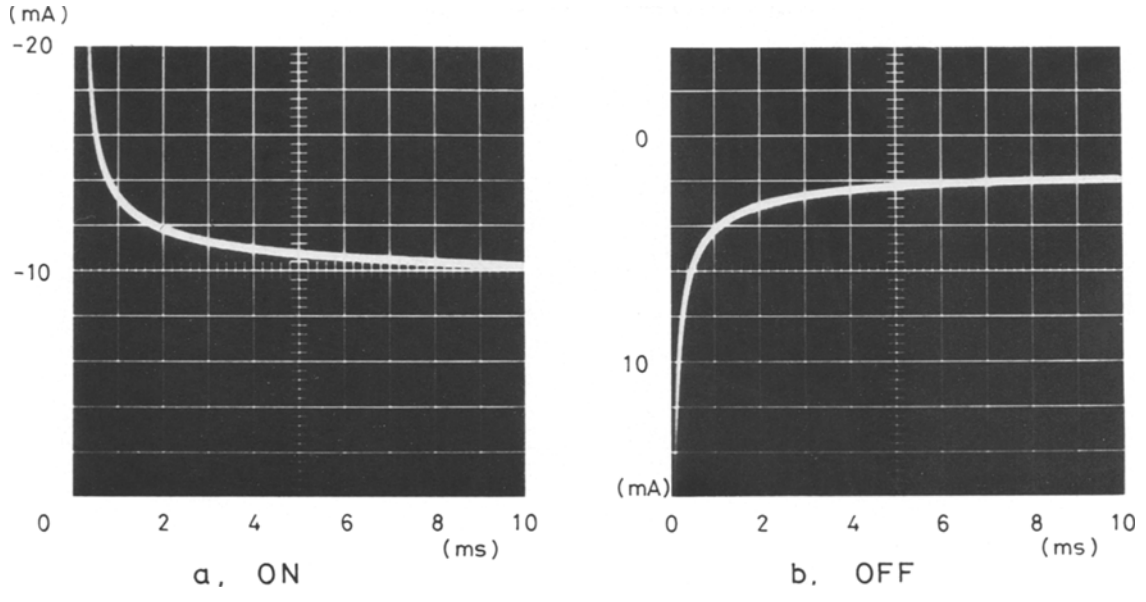

Fig. 2. Typical current transients on an oscilloscope 0.5 mol dm^{-3} $CuSO_4$ + 2.0 mol dm^{-3} H_2SO_4, $\eta = -60$ mV.

$$N_2 = \frac{l^2}{Dc_0}\frac{i_0}{zF}\left[\frac{\theta_0}{1-\theta_0}\exp\left(-\frac{\alpha_c F}{RT}\eta\right) + \exp\left(\frac{\alpha_a F}{RT}\eta\right)\right] \tag{1}$$

N_2 characterizes the behaviours of i/i_∞ which are given by Equations 2 and 3 for the ad-species, ad-atom Cu^0 and ad-ion Cu^+, respectively:

$$\frac{J}{J_\infty} = \frac{i}{i_\infty} = 1 + \frac{2N_2^{3/2}}{\tanh N_2^{1/2}} \sum_{n=0}^{\infty} \frac{\exp\left\{-\left[N_2 + \frac{(2n+1)^2\pi^2}{4}\right]T\right\}}{\frac{(2n+1)^2\pi^2}{4}\left[N_2 + \frac{(2n+1)^2\pi^2}{4}\right]} \tag{2}$$

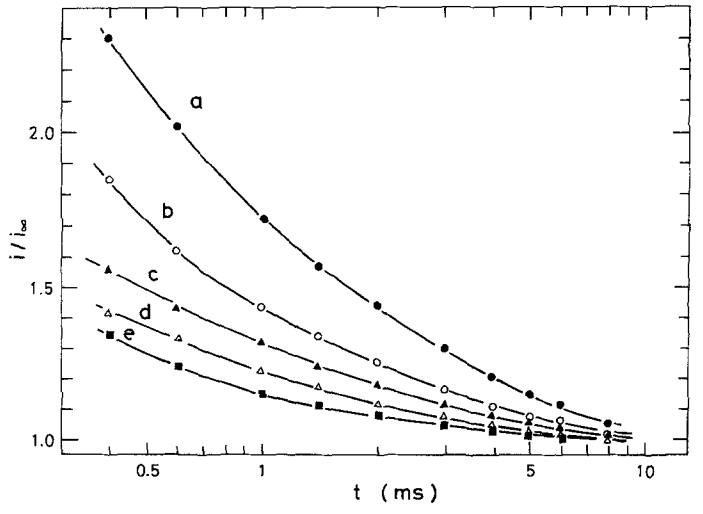

Fig. 3. Cathodic current transients in 0.5 mol dm^{-3} $CuSO_4$ + 2.0 mol dm^{-3} H_2SO_4. (a) — 9 mV, (b) — 18 mV, (c) — 54 mV, (d) — 69 mV, (e) —102 mV.

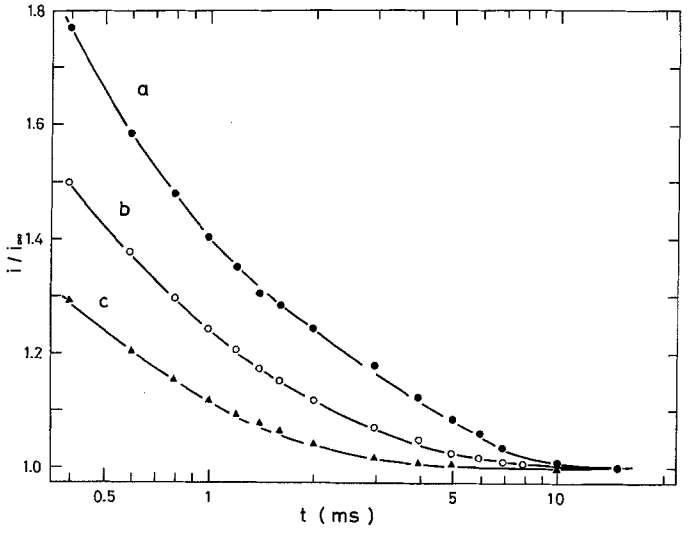

Fig. 4. Anodic current transients in 0.5 mol dm^{-3} $CuSO_4$ + 2.0 mol dm^{-3} H_2SO_4. (a) + 10 mV, (b) + 25 mV, (c) + 44 mV.

$$\frac{J}{J_\infty} = \frac{i}{i_\infty} = 1 + \frac{N_2^{1/2}}{\tanh N_2^{1/2}} \sum_{n=0}^{\infty} \frac{\left[N_2 - \dfrac{(2n+1)^2\pi^2}{4}\right]}{\dfrac{(2n+1)^2\pi^2}{4}\left[N_2 + \dfrac{(2n+1)^2\pi^2}{4}\right]} \exp\left\{-\left[N_2 + \frac{(2n+1)^2\pi^2}{4}\right]T\right\}. \quad (3)$$

The N_2 values are obtained as a function of overpotential by superimposing experimental i/i_∞ curves and theoretical J/J_∞ curves as shown in Fig. 5. The results show that N_2 has a maximum near the equilibrium potential and decreases with increasing cathodic and anodic overpotentials. This behaviour opposite to that expected theoretically at least at overpotentials greater than 20 mV.

It was seen that there was a resemblance between the shapes of the ON (deposition) and OFF (return to zero overpotential) curves. Figure 6 compares current-time curves. In the previous study the transient parts of the dimensionless currents were expressed as follows:

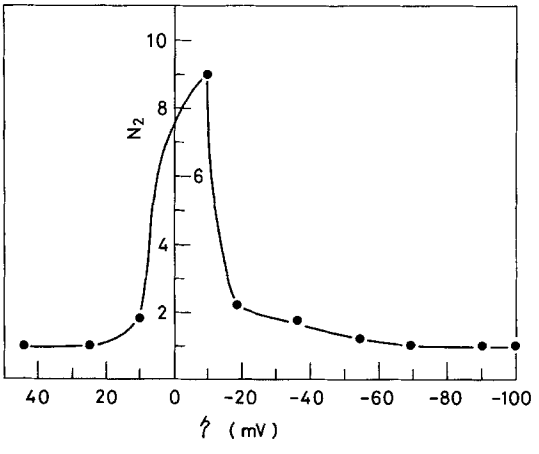

Fig. 5. Overpotential dependence of N_2 in 0.5 mol dm^{-3} $CuSO_4$ + 2.0 mol dm^{-3} H_2SO_4.

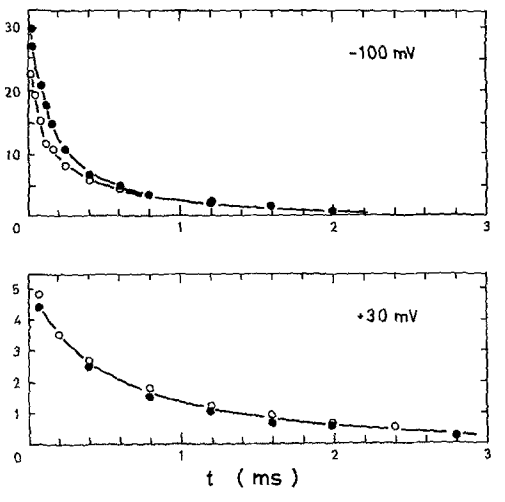

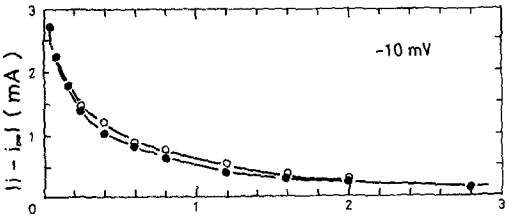

Fig. 6. Comparison of transient currents during ON and OFF in 0.5 mol dm^{-3} $CuSO_4$ + 2.0 mol dm^{-3} H_2SO_4. •: ON, ○: OFF.

Ad-atom Cu^0 as ad-species,

$$J'_{ON} = \sum_{n=0}^{\infty} \frac{8(N_1 - N_2)N_2}{(2n+1)^2\pi^2\left[N_2 + \dfrac{(2n+1)^2\pi^2}{4}\right]} \exp\left\{-\left[N_2 + \frac{(2n+1)^2\pi^2}{4}\right]T\right\} \tag{4}$$

and

$$J_{OFF} = \sum_{n=0}^{\infty} \frac{8N_3(N_2 - N_1)}{(2n+1)^2\pi^2\left[N_2 + \dfrac{(2n+1)^2\pi^2}{4}\right]} \exp\left\{-\left[N_3 + \frac{(2n+1)^2\pi^2}{4}\right]T\right\} \tag{5}$$

where

$$N_3 = \frac{i_0 l^2}{zFDc_0} \tag{6}$$

Ad-ion Cu^+ as ad-species,

$$J'_{ON} = \sum_{n=0}^{\infty} \frac{8(N_1 - N_2)\left[N_2 - \dfrac{(2n+1)^2\pi^2}{4}\right]}{(2n+1)^2\pi^2\left[N_2 + \dfrac{(2n+1)^2\pi^2}{4}\right]} \exp\left\{-\left[N_2 + \frac{(2n+1)^2\pi^2}{4}\right]T\right\} \tag{7}$$

$$J_{OFF} = \sum_{n=0}^{\infty} \frac{8(N_2 - N_1)\left[N_3 - \dfrac{(2n+1)^2\pi^2}{4}\right]}{(2n+1)^2\pi^2\left[N_2 + \dfrac{(2n+1)^2\pi^2}{4}\right]} \exp\left\{-\left[N_3 + \frac{(2n+1)^2\pi^2}{4}\right]T\right\}. \tag{8}$$

The ratio of the transients for ON and OFF can, at short times, be expressed in the following equations:

Ad-atom Cu^0 as ad-species,

$$\frac{i'_{ON}}{i_{OFF}} = \frac{J'_{ON}}{J_{OFF}} = -\frac{N_2}{N_3} = -\left[\frac{\theta_0}{1-\theta_0}\exp\left(-\frac{\alpha_c F}{RT}\right) + \exp\left(\frac{\alpha_a F}{RT}\right)\right] \tag{9}$$

Table 1. Initial current ratios of non-steady parts ON and OFF, J'_{ON}/J_{OFF}, calculated using Equation 10

	N_2					
N_3	0.1	1	5	10	20	100
1	− 1.4	− 1	+ 0.42	+ 1.6	+ 3.1	+ 8.6
10	+ 0.41	+ 0.32	− 0.19	− 1	− 3.3	-
100	+ 0.030	+ 0.022	− 0.012	− 0.057	− 0.15	− 1

Ad-ion Cu^+ as ad-species,

$$\frac{i'_{ON}}{i_{OFF}} = \frac{J'_{ON}}{J_{OFF}} = -\frac{\sum_{n=0}^{\infty}\left[N_2 - \frac{(2n+1)^2\pi^2}{4}\right] \Big/ (2n+1)^2\pi^2\left[N_2 + \frac{(2n+1)^2\pi^2}{4}\right]}{\sum_{n=0}^{\infty}\left[N_3 - \frac{(2n+1)^2\pi^2}{4}\right] \Big/ (2n+1)^2\pi^2\left[N_2 + \frac{(2n+1)^2\pi^2}{4}\right]}. \tag{10}$$

It is obvious that Equation 9 could not give the form observed when the ON and OFF curves are compared. Some calculations using Equation 10 are shown in Table 1. The results show that similar ON and OFF curves can be observed only under limited conditions. This is also the case for an ad-atom, as can be seen easily from Equation 9.

The foregoing results do not favour the surface diffusion model. For the model, surface diffusion penetration is given by [9]

$$\lambda_0 = \left(\frac{zFDc_0}{i_0}\right)^{1/2} \exp\left(-\frac{\alpha_a F}{2RT}\eta\right). \tag{11}$$

The criterion determining whether surface diffusion contributes to the rate controlling step was considered to be the value of λ_0/l, that is, the effect of surface diffusion is important when $\lambda_0/l \ll 1$. The order of magnitude of λ_0 is 10^{-6} cm using Equation 11 for both the ad-atom and ad-ion as the ad-species, even when one takes values for the parameters which make λ_0 small, that is, $D = 10^{-6}\,cm^2\,s^{-1}$, $i_0 = 0.1\,A\,cm^{-2}$, $c_0 = 10^{-10}\,mol\,cm^{-2}$ and a potential range of + 40 mV to − 100 mV. In the present study, the copper electrode was considered to have a dislocation density of the order of $10^{10}\,cm^{-2}$, since it was cold-rolled and no heat treatment was carried out. It could be valid to consider that dislocations function as steps at which ad-speices are incorporated into the lattice of the electrode [7], so the average distance between the steps is assumed to be of the order of 10^{-5} cm. This leads to a value of λ_0/l which could not always satisfy the condition that λ_0/l should be less than unity. It should be noted also that the above values of the parameters were estimated in order to make λ_0/l small.

In theoretical treatments, the variation of current with time becomes small if $T \geqslant 1$ ($T = Dt/l^2$). The corresponding t value is in the range 10^{-8} to 10^{-4} s, assuming $D = 10^{-5}$–$10^{-6}\,cm^2\,s^{-1}$ and $l = 10^{-5}$ cm. Consequently, measurements were performed in a much longer time range (up to 1.5×10^{-2} s) than that for surface diffusion behaviour. The above considerations imply the measurements using polycrystalline electrodes with a time period of milliseconds would not give us adequate information about surface diffusion.

3.2. *The direct incorporation model at hemispherical sites*

It was shown in the previous section that the surface diffusion model could not be applied to the present study. Therefore, other reasons for the current–time behaviour must be considered. These may include a geometric change of the electrode area [1, 2], bulk diffusion or some other factor. The first possibility may be rejected because of the small amount of deposition which occurs during the electrodeposition

period which is at most 10^{-3} C cm^{-2} for 1.5×10^{-2} s. This would be possible for an electrode with a very smooth surface, but the electrode used in the present study was polycrystalline and had undergone pre-electrodeposition treatment. Therefore, the state of the surface was considered to be 'rough' and the quantity of deposition could not cause a change of the actual surface area. Moreover, appreciable current decreases were observed even at low overpotentials and the solutions used had relatively high concentrations of cupric ion; therefore, bulk diffusion could not explain the behaviour in the low overpotential region. Hence, other causes of the current–time behaviour were considered.

3.2.1. Theory. Fleischmann and Harrison [10] have suggested a direct incorporation model. They considered the incorporation of metal ions discharged at point sites through hemispherical diffusion zones preceded by the usual linear diffusion. In the present study, hemispherical sites of finite size were considered to be the sites at which the incorporation of atoms takes place rather than point sites, and linear diffusion was neglected.

The model is shown in Fig. 7. A cupric ion arrives at the electrode through a diffusion layer with thickness $r_1 - r_0$ and undergoes charge transfer. Then, it is incorporated into the substrate. The diffusion equation and conditions are

$$\frac{\partial c}{\partial t} = D\left(\frac{\partial^2 c}{\partial r^2} + \frac{2\partial c}{r\partial r}\right). \tag{12}$$

The initial and boundary conditions are:

$$t = 0, \quad r_0 \leqslant r \leqslant r_1; \quad c = c_0 \tag{13}$$

$$t > 0, \quad r = r_1; \quad c = c_0 \tag{14}$$

$$r = r_0; \quad \frac{\partial c}{\partial r} = \frac{i_0}{zFDc_0}\left[c_s \exp\left(-\frac{\alpha_c F}{RT}\eta\right) - c_0 \exp\left(\frac{\alpha_a F}{RT}\eta\right)\right] = h(c_s - c_1) \tag{15}$$

where

$$h = \frac{i_0}{zFDc_0} \exp\left(-\frac{\alpha_c F}{RT}\eta\right) \tag{16}$$

$$c_1 = c_0 \exp\left[\frac{(\alpha_c + \alpha_a)F}{RT}\eta\right]. \tag{17}$$

It should be noted that D refers not to surface diffusion but to diffusion of cupric ions in solution. c_0 and c_s represent concentrations of cupric ion in the bulk solutions and at the surface of hemispherical sites, respectively, and the other notations are as usual. Current density, based on smooth unit area, is given by Equation 18.

$$i = i_0 S\left[\frac{c_s}{c_0} \exp\left(-\frac{\alpha_c F}{RT}\eta\right) - \exp\left(\frac{\alpha_a F}{RT}\eta\right)\right] \tag{18}$$

where S is roughness factor and dimensionless.

$$S = 2\pi m r_0^2 \tag{19}$$

where m is the number of hemispherical sites per cm^2. By taking $T = Dt/(r_1 - r_0)$, $X = (r_1 - r)^2/(r_1 - r_0)$ and $U = (c - c_0)r_0/c_0(r_1 - r_0)$, Equations 12 to 15 become

$$\frac{\partial U}{\partial T} = \frac{\partial^2 U}{\partial X^2} \tag{20}$$

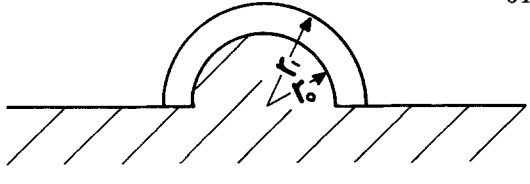

Fig. 7. Schematic diagram of the direct incorporation model at a hemispherical site.

with initial and boundary conditions;

$$T = 0, \quad 0 \leqslant X \leqslant 1; \quad U = 0 \tag{21}$$

$$T > 0, \quad X = 0; \quad U = 0 \tag{22}$$

$$X = 1; \quad \frac{\partial U}{\partial X} + h'(U + A) = 0 \tag{23}$$

where

$$h' = \frac{(1 + r_0 h)(r_1 - r_0)}{r_0} \tag{24}$$

and

$$A = \frac{r_0^2 h(c_0 - c_1)}{(r_1 - r_0)(1 + r_0 h)c_0} \tag{25}$$

The solution is [11]

$$U = \frac{-h'AX}{(1 + h')} + 2h'A \sum_{n=1}^{\infty} \frac{\sin(\beta_n X)}{(h' + h'^2 + \beta_n^2)\sin\beta_n} \exp(-\beta_n^2 T) \tag{26}$$

where $n = 1, 2, 3 \ldots$ are the positive roots of

$$\beta \cot\beta + h' = 0. \tag{27}$$

The surface concentration, c_s is given by

$$c_s = \frac{c_0(r_1 - r_0)}{r_0} U|_{X=1} + c_0 \tag{28}$$

c_s can be expressed as Equation 29 since Equation 26 gives $U|_{X=1}$.

$$c_s = c_0 - \left(\frac{c_0(r_1 - r_0)}{r_0}\right)\left(\frac{h'A}{1 + h'}\right) + \frac{c_0(r_1 - r_0)}{r_0} 2h'A \sum_{n=1}^{\infty} \frac{\exp(-\beta_n^2 T)}{h' + h'^2 + \beta_n^2}. \tag{29}$$

Consequently, current density is given by

$$i = \left(\frac{zFSDc_0 r_1}{r_0^2}\right)\left(\frac{h'A}{1 + h'}\right) + \frac{2zFSDc_0}{r_0} h'A\left[h' - \frac{(r_1 - r_0)}{r_0}\right] \sum_{n=1}^{\infty} \frac{\exp(-\beta_n^2 T)}{h' + h'^2 + \beta_n^2}. \tag{30}$$

3.2.2. Steady-state conditions. Steady-state current density i_∞ is deduced from Equation 30,

$$i_\infty = \frac{zFDSr_1(c_0 - c_1)h}{r_0 + r_0 r_1 h - r_0^2 h}. \tag{31}$$

This expression can be converted in to the form of Equation 33 by using Equation 32,

$$\frac{h'A}{1 + h'} = -U_\infty|_{X=1} \tag{32}$$

$$i_\infty = \left(\frac{zFSD(c_0 - c_{s\infty})}{r_1 - r_0}\right)\left(\frac{r_1}{r_0}\right). \tag{33}$$

When $r_1 = r_0$ that is, the thickness of the diffusion layer is zero and charge transfer is the rate determining step, the steady-state current density is reduced to the usual Butler–Volmer equation,

$$i_\infty = i_0 S\left[\exp\left(-\frac{\alpha_c F}{RT}\eta\right) - \exp\left(\frac{\alpha_a F}{RT}\eta\right)\right]. \tag{34}$$

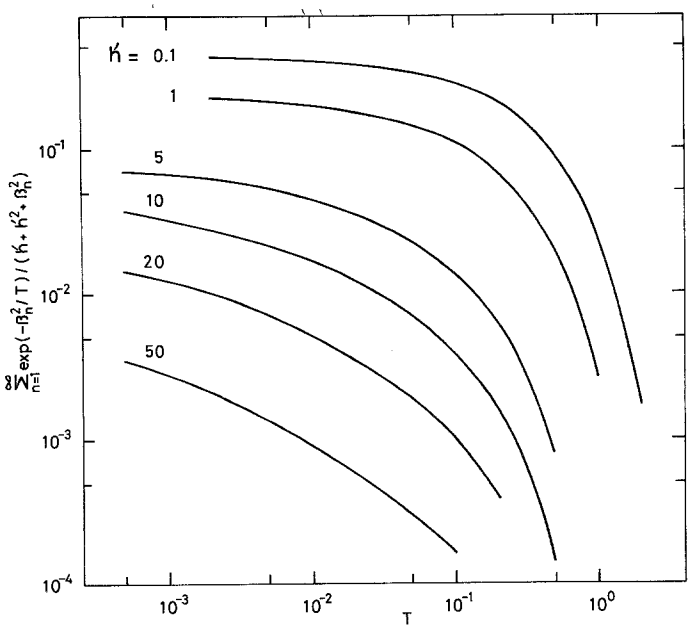

Fig. 8. Transients of $\Sigma_{n=1}^{\infty} \exp(-\beta_n^2/T)/(h' + h'^2 + \beta_n^2)$ at various h' values.

On the other hand, in the case of $r_1 \gg r_0$, Equation 33 becomes Equation 35,

$$i_\infty = zFSD(c_0 - c_{s\infty})\left(\frac{1}{r_0}\right). \tag{35}$$

This expression is similar to the one for semi-infinite spherical diffusion [12].

Here, a comparison with experimental results is not given, because it is uncertain which value of current density should be chosen as the steady-state value. During electrodeposition, the area of the electrode surface changes, and it seems invalid to use the current obtained after a long time as the steady-state value which pertains to a particular surface area.

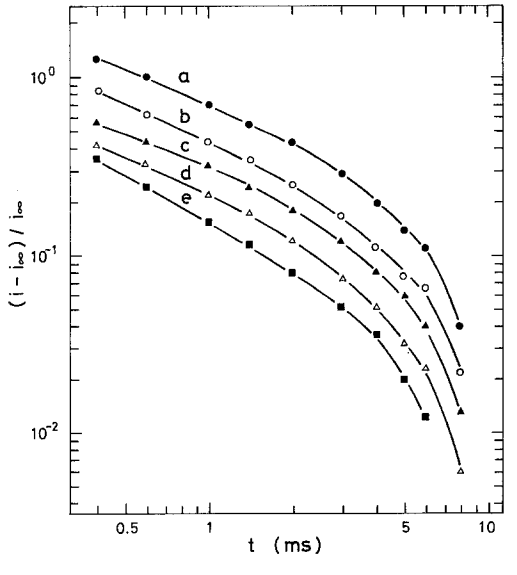

Fig. 9. Transients of $(i - i_\infty)/i_\infty$ in 0.5 mol dm^{-3} $CuSO_4$ + 2.0 mol dm^{-3} H_2SO_4 (a) $\eta = -9$ mV, (b) -18 mV, (c) -54 mV, (d) -69 mV, (e) -102 mV.

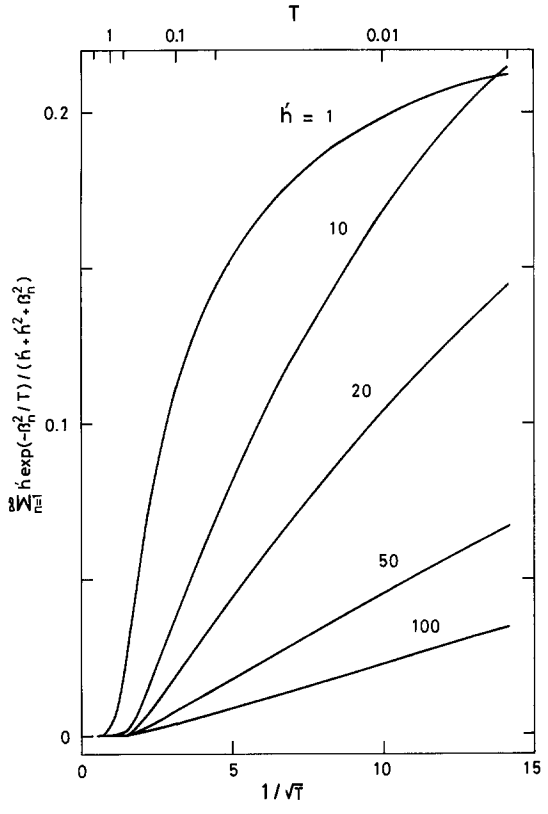

Fig. 10. Plots for $\Sigma_{n=1}^{\infty} h' \exp(-\beta_n^2 T)/(h' + h'^2 + \beta_n^2)$ against $1/T^{1/2}$ at various h' values.

3.2.3. Current–time behaviour. Equation 30 gives transient $(i - i_\infty)/i_\infty$.

$$\frac{i - i_\infty}{i_\infty} = \frac{2(h' - R)(1 + h')}{R + 1} \sum_{n=1}^{\infty} \frac{\exp(-\beta_n^2 T)}{h' + h'^2 + \beta_n^2} \tag{36}$$

where

$$R = \frac{r_1 - r_0}{r_0}. \tag{37}$$

The transient behaviour of $(i - i_\infty)/i_\infty$ can be represented by $\Sigma_{n=1}^{\infty} \exp(-\beta_n^2/T)/(h' + h'^2 + \beta_n^2)$ if the

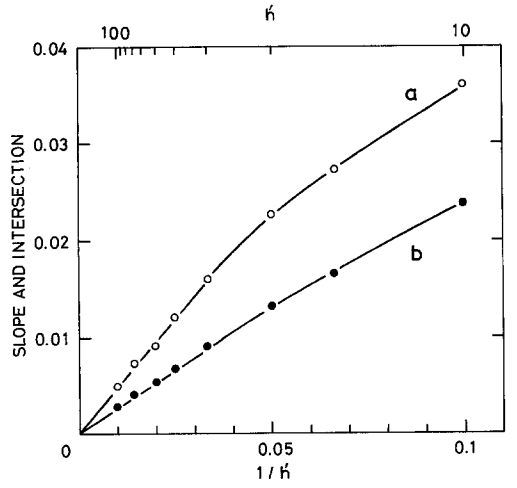

Fig. 11. Slopes and intersections at $1/T^{1/2} = 0$ obtained from the plots in Fig. 10 against $1/h'$ (a) slopes, (b) intersections

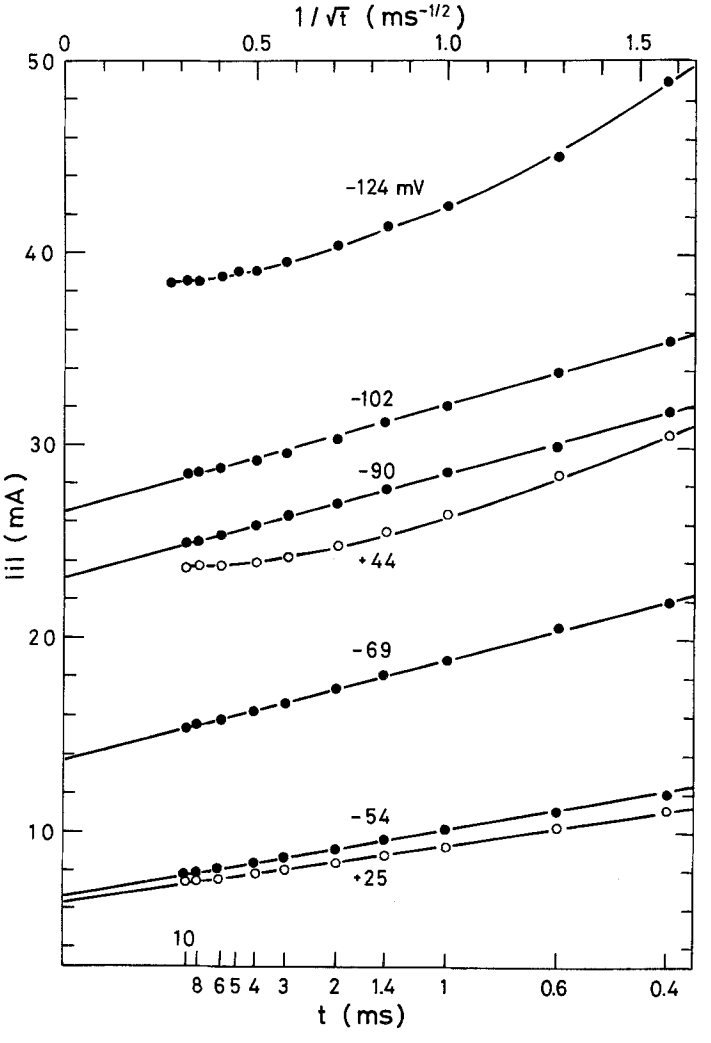

Fig. 12. Current against $1/t^{1/2}$ in 0.5 mol dm^{-3} $CuSO_4$ + 2.0 mol dm^{-3} H_2SO_4.

size of the hemispherical site and the thickness of the diffusion layer do not change during the ON time. Some transients of $\Sigma_{n=1}^{\infty} \exp(-\beta_n^2 T)/(h' + h'^2 + \beta_n^2)$ are calculated for various h' values in Fig. 8. Equivalent plots can be obtained from the experimental results (Fig. 9). The results show a similar behaviour to the theoretical curves. On comparison of the experimental and theoretical curves, the time range measured in the experiments is consistent with the T range of 0.01 to 1 for the theoretical curves.

Then, plots of $\Sigma_{n=1}^{\infty} h' \exp(-\beta_n^2 T)/(h' + h'^2 + \beta_n^2)$ against $1/T^{1/2}$ are shown in Fig. 10. The relationship is linear in the region $h' > 20$ and $T = 0.01$–1. Plots of the slopes and intersections, with $1/T^{1/2} = 0$, against $1/h'$ are also linear as shown in Fig. 11. As a result of the two linear relationships, the function $\Sigma_{n=1}^{\infty} h' \exp(-\beta_n^2 T)/(h' + h'^2 + \beta_n^2)$ can be converted to the form of Equation 38 as an approximate equation using the slopes of the lines with $h' > 20$:

$$\sum_{n=1}^{\infty} \frac{h' \exp(-\beta_n^2 T)}{h' + h'^2 + \beta_n^2} = -\frac{0.47}{h'} + \frac{0.26}{h' T^{1/2}}. \tag{38}$$

The approximate equation for current density is

$$i = \frac{zFSDh(c_0 - c_1)}{r_1 + r_1 r_0 h + r_0^2 h} - \frac{2 \times 0.47 zFSDr_0^2 h^2 (c_0 - c_1)}{(r_1 - r_0)(1 + r_0 h^2)} + \frac{2 \times 0.26 zFS D^{1/2} r_0^2 h^2 (c_0 - c_1)}{(1 + r_0 h)^2 t^{1/2}} \tag{39}$$

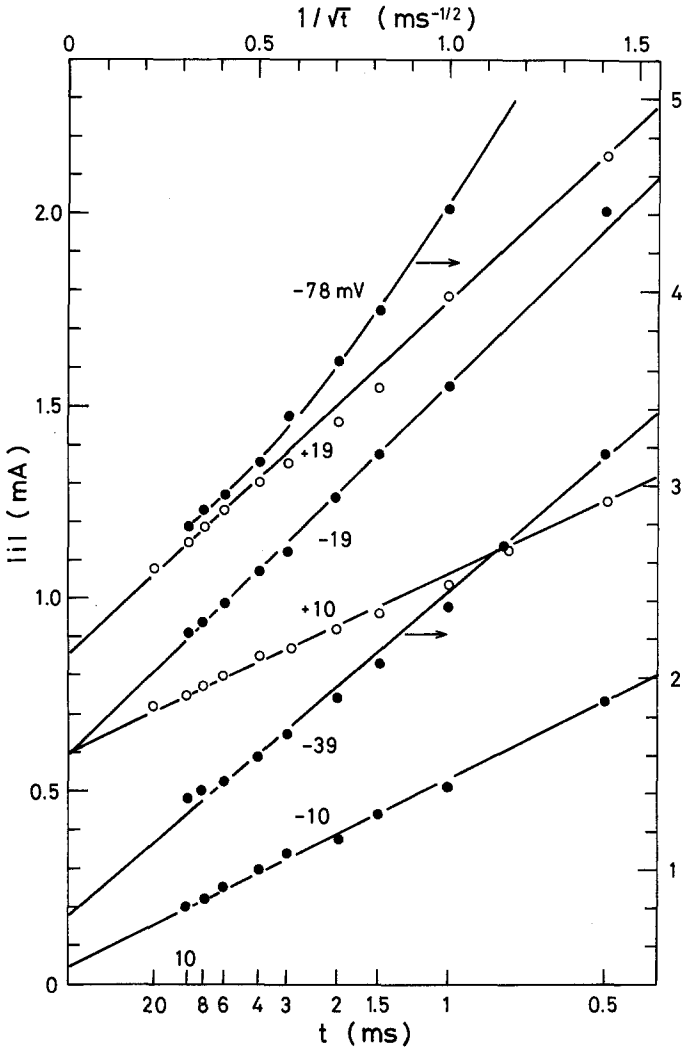

Fig. 13. Current against $1/t^{1/2}$ in 0.05 mol dm^{-3} $CuSO_4$ + 0.5 mol dm^{-3} H_2SO_4.

This equation implies a linear relationship between current density and $1/t^{1/2}$. These are plotted for experimental results in two aqueous solutions in Figs. 12 and 13. Fairly good linearity is obtained with relatively low overpotentials, but a deviation from linearity occurs in the high overpotential region. The results seem to suggest that the direct incorporation model is applicable at low overpotentials but that it cannot hold at high overpotentials where bulk diffusion becomes predominant.

Some parameters can be estimated from Equation 39. The slope and the difference between the intersection at $1/T^{1/2} = 0$ and the steady-state current density from the experimental plot could give the third and second terms in Equation 39. As mentioned before, the true steady-state current density cannot be obtained. The only available quantity is the slope. If $r_0 h \ll 1$, the slope is expressed as in Equation 40 from the third term in Equation 39.

$$\frac{0.26(i_0 S)^2}{\pi z F D^{3/2} c_0 m}\left\{\exp\left(-\frac{2\alpha_c F}{RT}\eta\right) - \exp\left[\frac{(\alpha_a - \alpha_c)F}{RT}\eta\right]\right\}. \tag{40}$$

The assumption that $r_0 h \ll 1$ is appropriate because the values of h are of the order of 10^{-2} to 10^{-3} for the overpotential range applied. The number of sites per unit area can be obtained using the values $z = 2, \alpha_c = 0.5, \alpha_a = 1.5, D = 7.2 \times 10^{-6}$ cm^2 s^{-1} and $i_0 = 3 \times 10^{-3}$ A cm^{-2} for 0.5 mol dm^{-3} $CuSO_4$

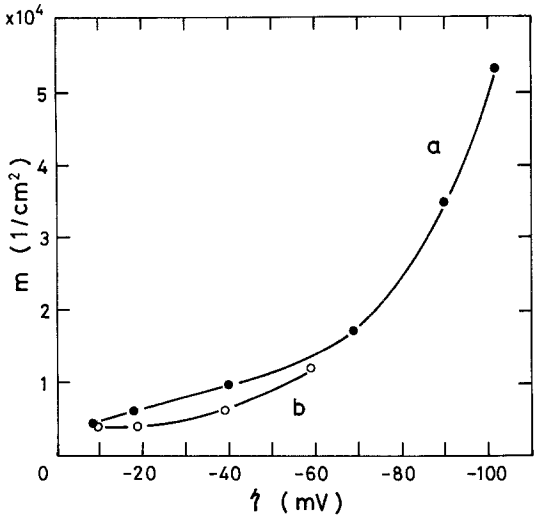

Fig. 14. Overpotential dependence of the numbers of hemispherical sites, m, (a) 0.5 mol dm^{-3} $CuSO_4$ + 2.0 mol dm^{-3} H_2SO_4, (b) 0.05 mol dm^{-3} $CuSO_4$ + 0.5 mol dm^{-3} H_2SO_4.

solution and 4×10^{-4} A cm^{-2} for 0.05 mol dm^{-3} $CuSO_4$ solution. Fig. 14 shows the dependence of m on overpotential. In the figure only points which satisfy linearity were plotted. The value was of the order of 10^4 cm^{-2} and increased with overpotential. No significant difference was observed between the two solutions with different $CuSO_4$ concentrations. If a single potential pulse was utilized for the measurements, no potential dependence of m might be expected. In the present study, however, a continuous pulse was applied instead of a single pulse and measurements of current–time behaviour were performed 5 to 10 min after applying the continuous pulse. Therefore, the period of the pulse would affect the results more at high overpotentials than at low overpotentials because of the high current passed and in consequence the increased charge at high overpotentials. This seems to be a cause of the sudden increase of m at high overpotentials.

As mentioned above, current transients appeared at short times for electrodeposition in solutions with relatively high $CuSO_4$ concentrations. Hence, with polycrystalline copper electrodes the transients seemed to be caused by direct incorporation into hemispherical sites preceded by hemispherical diffusion rather than surface diffusion or an area change of the electrode.

References

[1] I. R. Burrows, J. A. Harrison and J. Thompson, *J. Electroanal. Chem.* 58 (1975) 241.
[2] J. A. Harrison and P. J. Stronach, *J. Electroanal. Chem.* 72 (1976) 239.
[3] A. Damjanovic, T. H. Setty and J. O'M. Bockris, *J. Electrochem. Soc.* 113 (1966) 429.
[4] M. Fleischmann and H. R. Thirsk, *Electrochim. Acta* 2 (1960) 22.
[5] M. Fleischmann, S. K. Rangarajan and H. R. Thrisk, *Trans. Faraday Soc.* 63 (1967) 1240.
[6] J. A. Harrison, *J. Electroanal. Chem.* 18 (1968) 18.
[7] A. Damjanovic and J. O'M. Bockris, *J. Electrochem. Soc.* 110 (1963) 1035.
[8] Y. Ogata, K. Yamakawa and S. Yoshizawa, *J. Appl. Electrochem.* submitted.
[9] K. J. Vetter, 'Electrochemical Kinetics', Academic Press, New York (1967) p. 287.
[10] M. Fleischmann and J. A. Harrison, *Electrochim. Acta* 11 (1966) 749.
[11] H. S. Carslaw and J. C. Jeager, 'Conduction of Heat in Solids', Oxford University Press, London (1959) p. 125.
[12] P. Delahay, 'New Instrumental Methods in Electrochemistry', Interscience, New York (1954) p. 61.